Sentinel-1 mission: results of the InSARap project

Matteo Nannini, Pau Prats–Iraola, Rolf Scheiber, Nestor Yague–Martinez   German Aerospace Center (DLR), Germany, matteo.nannini@dlr.de

Federico Minati, Francesco Vecchioli, Mario Costantini   e-GEOS SpA, ASI/Telespazio, Italy

Sven Borgstrom, Prospero De Martino, Valeria Siniscalchi   National Institute of Geophysics and Volcanology (INGV), Vesuvius Observatory, Italy

Thomas Walter,   German Research Centre for Geosciences (GFZ), Germany

Michael Foumelis,   RSAC c/o ESA-ESRIN, EO Science, Applications and Future Technologies Department, Italy

Yves-Louis Desnos,   ESA-ESRIN, EO Science, Applications and Future Technologies Department, Italy

Abstract

This paper analyzes the interferometric performance of the Sentinel-1 sensor, by presenting some of the many highlights of the first one and a half years of operation of the mission. The analysis has been carried out as part of the ESA-funded InSARap project. The paper will focus on persistent scatterer interferometric results and their validation, as well as on the analysis of selected events, namely, the Fogo volcano and the Gorkha Earthquake. Moreover, the applicability of SAR tomography to Sentinel-1 data is also demonstrated.

1   Introduction

The European Space Agency's (ESA) Sentinel-1A satellite was successfully launched on April 3rd, 2014. Its main operational mode, the Interferometric Wide swath (IW) mode operated as TOPS mode, provides a large swath width of 250 km at a ground resolution of 5mx20m in range and azimuth, respectively [9]. Due to the large coverage of the sensor, strong interest has been shown in determining the corresponding interferometric performance. In this sense, ESA funded the InSARap studies [3] as part of the SEOM activities of the Copernicus Programme. It has been shown that, despite the special characteristics of the TOPS mode, interferometry as well as time series analysis by means of PSI techniques could be reliably performed. The technical aspects related to a proper interferometric processing of TOPS data have been deeply analyzed in the past years leading to a solid processing strategy [7]. This paper presents the main PSI Sentinel-1 results over pilot sites like Mexico City and Campi Flegrei obtained with the DLR-HR TAXI PSI processor [4, 6, 8]. Results covering the eruption of the Fogo volcano and the Gorkha earthquake in Nepal will be shown as well. Moreover, in spite of the fact that Sentinel-1 has not been designed to suit SAR tomography due to the relatively small orbital tube (radius of 100 m), section 3 is dedicated to show a preliminary demonstration of the applicability of such technique for urban environment with Sentinel-1 data.

2   Sentinel-1 Interferometric Results

This section shows several results that demonstrate the excellent interferometric capabilities of Sentinel-1. Since the last change in the synchronization strategy on October 3rd, 2014, Sentinel-1 has been building up stacks very fast thanks to the 12 day repeat-pass and first time series results were presented at the InSARap [2] and Fringe [1] workshops by different independent groups. The Sentinel-1 performance in terms of burst mis-synchronization, Doppler centroid and perpendicular baseline, based on the analysis of more than 100 interferograms has shown the 1σ standard deviations for those parameters to be 1.8 ms, 20 Hz and 75 m, respectively. This results in a common azimuth bandwidth larger than 95% of the total one, while the range spectral shift is negligible due to the small orbital tube. These numbers confirm the excellent orbit and attitude control of Sentinel-1. These are essential prerequisites for achieving the excellent interferometric performance that will be shown in the following sections.

2.1   Campi Flegrei

For the pilot site of Campi Flegrei several configurations in ascending as well as descending geometry have been acquired by Sentinel-1.
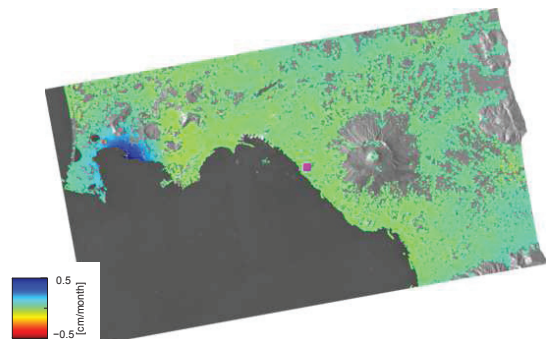

Figure 1: Deformation map for the ascending configuration over Campi Flegrei obtained by DLR-HR TAXI DInSAR processor.

Due to lack of space only results concerning the as-

cending configuration will be reported. However, as we shall see in section 2.1.1, all the available configurations are combined to retrieve the motion vector components. The ascending stack is composed by 37 images acquired between October 20th, 2014 and February 12th, 2016. The DInSAR retrievals are represented in **Figure 1**. As expected the strongest deformation corresponds to the Campi Flegrei region in the gulf of Pozzuoli where a ground uplift up to 0.5 cm/month can be estimated. In-situ measurements have confirmed such results by evaluating the retrieved time series and comparing them with continuous GPS (cGPS) measurements. **Figure 2** reports some validation plots also for the retrieved easting and up component. The next section is dedicated to describe how the latter two contributions are obtained.
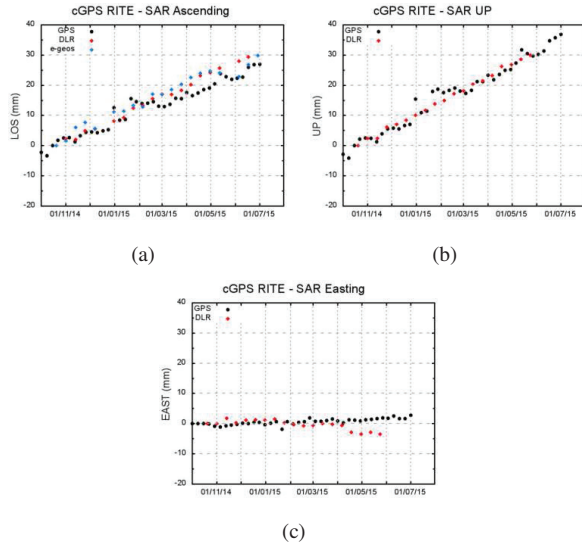

(a)   (b)

(c)

Figure 2: CGPS validation for the RITE station: (a) LOS, (b) vertical and (c) east components. The LOS comparison also present the cross-check between DLR's TAXI DInSAR chain and the e-Geos one.

2.1.1 Motion vector inversion

The SAR measurements obtained with differential SAR interferometry are related to the motion of the scene in the line-of-sight (LOS) direction of the satellite. In other words, the measured change corresponds to the dot product between the LOS vector and the motion vector. In order to retrieve the 3D motion vector it is necessary to have at least three independent LOS measurements, with the LOS vectors being as orthogonal as possible. In the case of SAR satellites flying in quasi-polar orbits, the LOS vector is in practice almost orthogonal to the north-south component, which results in DInSAR measurements almost insensitive to North-South motion. For this reason, in most cases only the Up and East components are inverted, since note that the inversion of the North one impairs mainly the inversion of the Up direction. The East component is the best constrained when using ascending and descending acquisitions. Therefore, having at least two configurations, it is possible to invert for Up

and East by solving a system of equations corresponding to the number of available geometries. **Figure 3** reports the estimated components for the common viewed area and shows, in addition to the expected deformation in the Up direction, also a relevant East/West component at the caldera. Indeed, there is also a non-negligible contribution in the North direction, but it is not possible to retrieve it due to the lack of sensitivity of the DInSAR phase to this component, as already explained. These results agree very well with the expected deformation as shown in **Figure 2**.
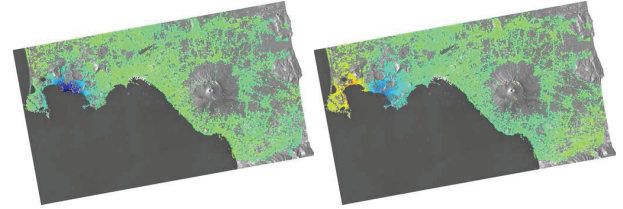

Figure 3: Result of the 2D inversion of the mean deformation velocity over the Campi Flegrei caldera using the three available configurations. (Left) Up and (right) East component. Scale as in **Figure 1**.

2.1.2 Exploitation of the Cross-Pol Channel

The Sentinel-1 satellite can be operated in the dual-pol mode by using the simultaneous dual-receive chain, hence allowing the acquisition of HH-HV or VV-VH channels. Different polarimetric channels can be exploited for example to increase the number of detected PS and hence improve the overall performance of the PSI chain [5]. In order to demonstrate this capability also with Sentinel-1, the two channels of the descending-2 acquisition over Campi Flegrei have been processed focusing on the area of Naples. As expected an increase in the PS density when combining the information of both channels results since most of the points are not common to both. In particular the number of detected PS has been of 655k and 425k for the VV and VH channels, respectively with 133k PS being the common ones.

2.2 Mexico City

This section is dedicated to analyze the results obtained over Mexico City. As is well known, the city is subject to strong subsidence (ca. 2 cm/month) as a consequence of ground water extraction. Due to the large swath coverage of Sentinel-1, Mexico City can be viewed with two different geometries for each ascending/descending configuration, since it is placed in the common overlap area of the swaths. This results in four data stacks of roughly 20 images each. Here, only the DInSAR retrieval for a descending configuration is reported (see **Figure 4**), where the area subject to the strongest deformation around the Mexico City International airport is easily identifiable in red. The processed data have been acquired from October 10th, 2014 and June 29th, 2015.
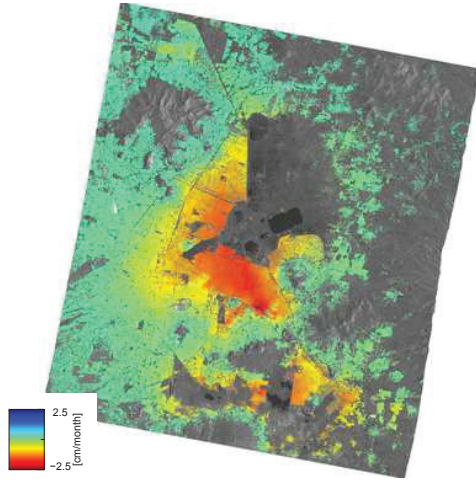
Figure 4: Deformation map for the descending configuration data over Mexico City obtained by DLR-HR TAXI DInSAR processor.

2.2.1 Cross-validation with Different Geometries

The four measurements of the same deformation pattern can be cross-compared to assess the performance of the PSI chain when working with Sentinel-1 data. In order to properly perform the comparison between the different geometries, it has been assumed that the deformation occurs only in the vertical direction. Therefore, prior to the comparison, the LOS deformation has been projected to the local Up component. **Figure 5** summarizes such analysis by means of histograms of the differences between the retrieved mean deformations.
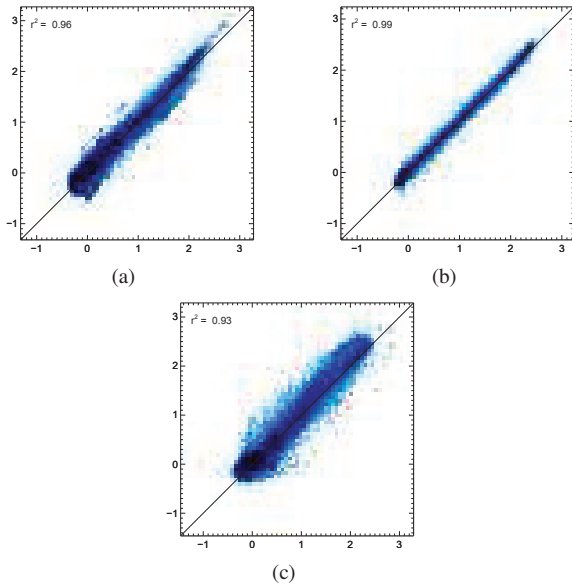

Figure 5: Cross-comparison between different geometries in cm/month. (a) ascending-1 vs ascending-2, (b) descending-1 vs descending-2 and (c) ascending-1 vs descending-2.

Now, since it has been observed that the larger APS noise is mainly present in the ascending configuration, one would expect that the comparison involving only ascending acquisitions to be the worst one, but this is not the case, since the ascending/descending comparison present a larger mismatch. To interpret this result it is worth reminding that the projection to the common vertical direction is correct if the scene is subject to vertical deformation only, while it can fail if some horizontal motion is present. This is indeed the case for the considered test site as will be shown in the following section, where a slight horizontal deformation component is detected. Therefore, the results of the cross-comparison are indeed consistent with the nature of the observed deformation and it can be concluded that the estimation carried out from the different geometries is consistent and do not present biases/trends of any kind. These results validate the processing strategy used to perform the interferometric processing [7].

2.2.2 Motion Vector Inversion

As already introduced in the previous section and as done for the Campi Flegrei site, different geometries can be combined to invert the 2D motion vector in the East and Up directions. Such result for Mexico City is shown in **Figure 6** detecting a clear non-negligible signal in the East deformation map. Note the different scales of the maps.
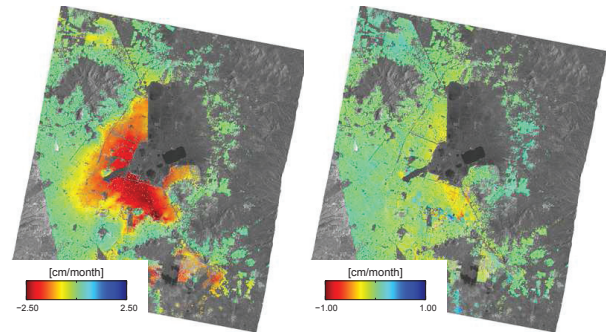

Figure 6: Result of the 2D inversion of the mean deformation velocity over Mexico City using three configurations. (Left) Up component and (right) East component.

2.3 Fogo Volcano

The eruption of the Fogo volcano on November 23rd, 2014, was the very first volcanic activity monitored by Sentinel-1. In spite of the challenging scene, the obtained interferogram is free of phase jumps thanks to the accurate InSAR processing. One InSAR pair for each descending and ascending configuration was processed and due to data modeling, a trending crack that opened at ∼1 km beneath the surface, responsible for 97% of the observed InSAR displacements, could be identified as shown in **Figure 7**.
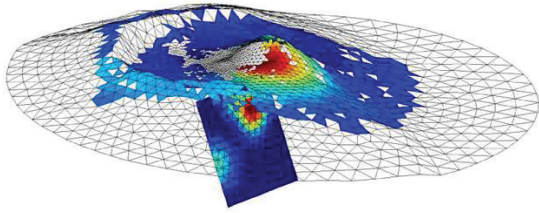
Figure 7: Sentinel-1 InSAR map draped over a digital elevation model and meshed by triangular elements.

2.4 The Gorkha Earthquake

On April 25th, 2015, a large earthquake hit Nepal, with the epicentre located 80 km northwest of Kathmandu. The earthquake was follow by several aftershocks, being the most relevant the one taking place on May 12th, 2015. In total, more than 9,000 people were killed and more than 23,000 were injured. Sentinel-1 data acquired over the area where processed and the scaled unwrapped differential interferogram is reported in **Figure 8**.
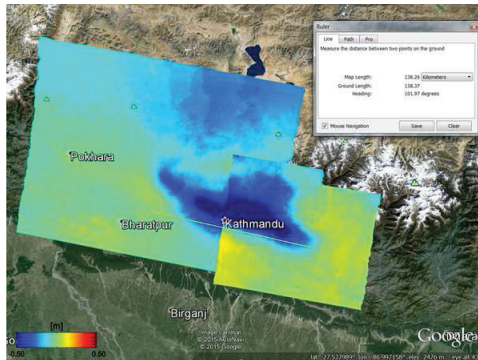

Figure 8: Nepal earthquake: scaled unwrapped phase overlaid overlay with Google image.

3 Tomography

SAR tomography is an imaging technique that allows the retrieval of the vertical distribution of scatterers sharing the same resolution cell. This is done by exploiting the resolution capabilities resulting from an aperture built in the perpendicular line-of-sight (PLOS) or cross-range direction. Such aperture can be sampled by means of repeated acquisitions with a varying baseline. The fact that Mexico City presents a skyline with several extremely tall buildings, make this particular test site the ideal candidate to first demonstrate the applicability of SAR tomography to Sentinel-1 data, despite the reduced orbital tube size. The Capon estimator is applied to the set of co-registered SLCs and a tomogram (azimuth-vertical slice) like the one reported in **Figure 9** can be produced. The layover between the scatterers located on the façade of the building and the ground is resolved and the highest tower of Mexico City, the Torre Mayor, can be easily identified. This preliminary analysis shows that for particular scenarios Sentinel-1 can suit SAR tomography.
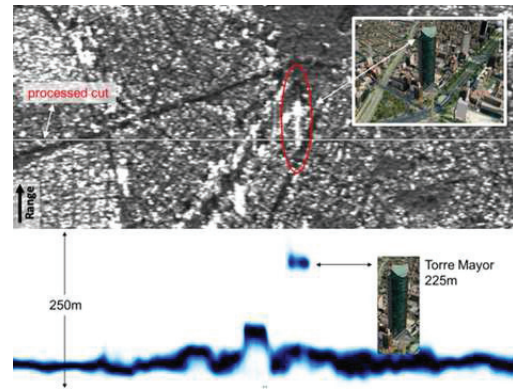

Figure 9: Sentinel-1 tomogram of the 225 m height Torre Mayor.

4 Conclusions

This paper reported some of the main highlights that could be achieved in the first one and a half years of operation of Sentinel-1. The excellent performance of the SAR sensor allowed a practically straightforward extension of the established interferometric techniques to Sentinel-1. The presented results demonstrate that the unique wide-swath capability offered by the TOPS mode for interferometric applications will allow present and future missions to improve the role of SAR remote sensing as an information retrieval tool.

References

[1] Fringe workshop,23–27 March 2015, Frascati, Italy. http://seom.esa.int/fringe2015/.

[2] InSARap workshop, 10–11 December 2014, Frascati, Italy. http://seom.esa.int/insarap/.

[3] InSAR Performance Study with TOPS Data. 2014. http://seom.esa.int/page_project006.php.

[4] Matteo Nannini et al. TOPS Time Series Performance Assessment With TerraSAR-X Data. *IEEE Journal of Selected Topics in Applied Earth Observations and Remote Sensing*, PP(99), 2016.

[5] V. D. Navarro-Sanchez and J. M. Lopez-Sanchez. Improvement of persistent-scatterer interferometry performance by means of a polarimetric optimization. *Geoscience and Remote Sensing Letters, IEEE*, 9(4):609–613, 2012.

[6] Pau Prats et al. TAXI: A versatile processing chain for experimental TanDEM-X product evaluation. In *2010 IEEE International Geoscience and Remote Sensing Symposium (IGARSS)*. IEEE, 2010.

[7] Pau Prats-Iraola et al. TOPS interferometry with TerraSAR-X. *IEEE Transactions on Geoscience and Remote Sensing*, 50(8):3179–3188, 2012.

[8] Pau Prats-Iraola et al. Sentinel-1 assessment of the interferometric wide-swath mode. In *2015 IEEE International Geoscience and Remote Sensing Symposium*. IEEE, 2015.

[9] Ramon Torres et al. GMES Sentinel-1 mission. *Remote Sensing of Environment*, 120:9–24, 2012.